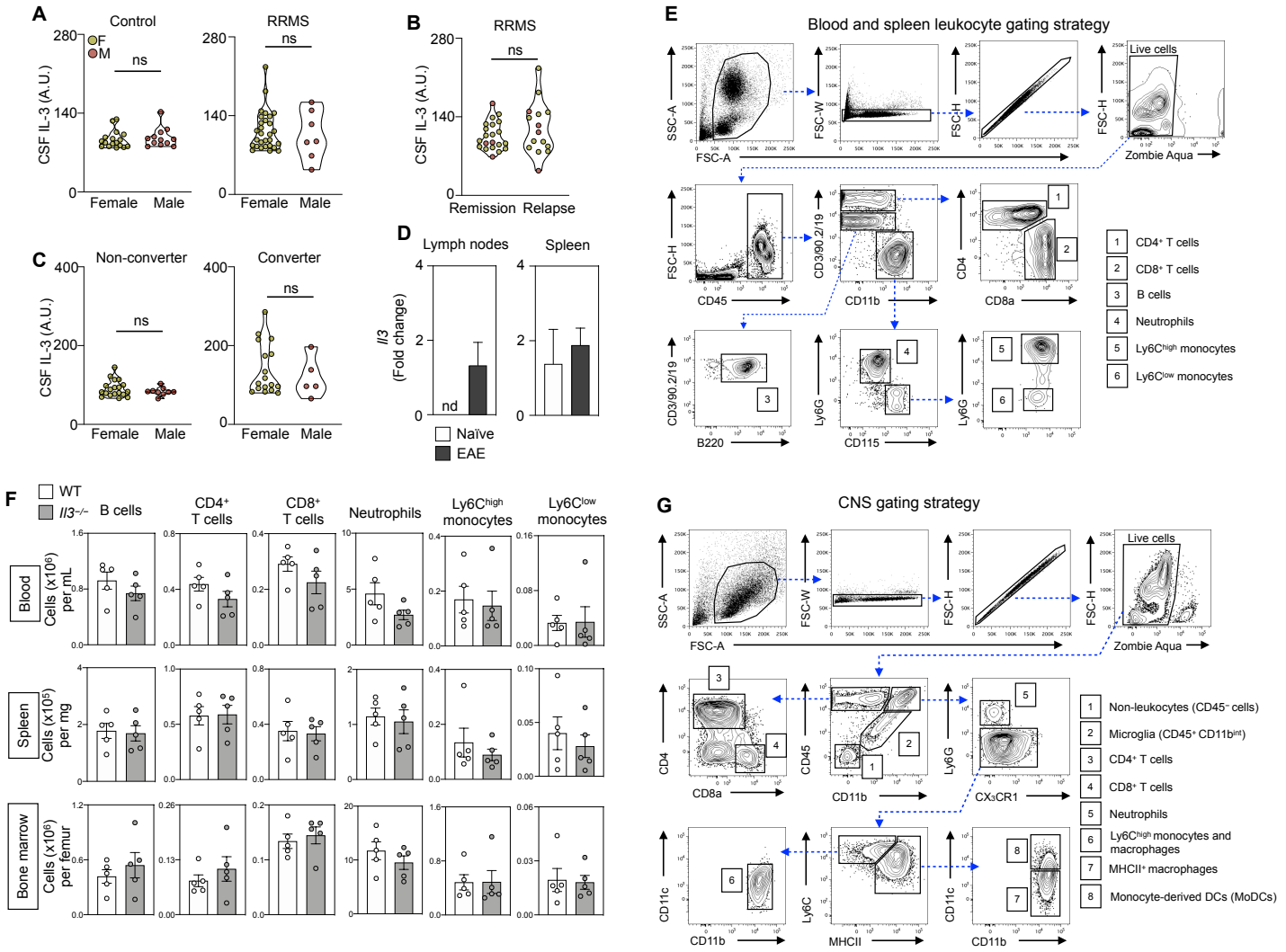

Figure S1. CSF IL-3 in RRMS and *Il3* expression, gating strategy and enumeration of leukocytes in WT and *Il3*$^{-/-}$ EAE mice.

(A) IL-3 amount in the CSF of male and female control and RRMS subjects (n=17 control females, 12 control males, 30 RRMS females, 7 RRMS males; Mann–Whitney *U*-tests).

(B) CSF IL-3 in male and female RRMS patients during relapse or remission (n=21 remission, 15 relapse; Mann–Whitney *U*-tests).

(C) CSF IL-3 amount in male and female converter and non-converter CIS patients (n=19 non-converter females, 9 non-converter males, 17 converter females, 5 converter males; Mann–Whitney *U*-tests).

(D) *Il3* expression in lymph nodes and spleen of control and EAE mice at peak (n=4-5 mice/group).

(E) Representative flow cytometric peripheral leukocyte gating strategy during the peak of EAE.

(F) Quantification of immune cell subsets in the blood, spleen, and bone marrow of WT and *Il3*$^{-/-}$ mice (n=5 mice/group).

(G) Representative flow cytometric CNS leukocyte gating strategy during the peak of EAE.

Mean±s.e.m.

CSF, cerebrospinal fluid; EAE, experimental autoimmune encephalomyelitis; ns, not significant.

Supplemental Figure 1 – related to Figure 1

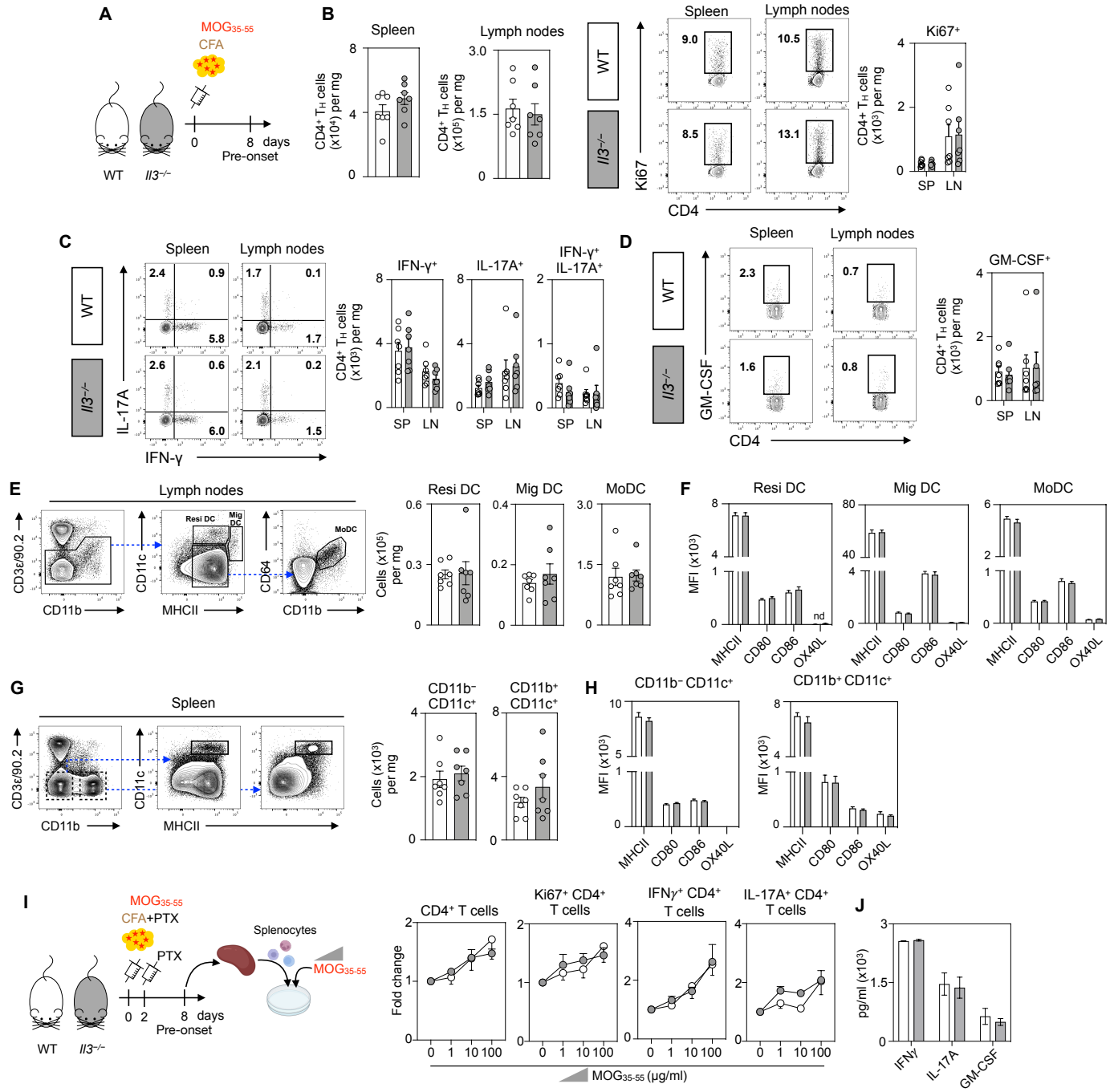

Figure S2. IL-3 is dispensable for the peripheral priming of myelin-reactive CD4⁺ T cells.
(A) Schematic diagram of the experimental design. WT and *Il3*$^{-/-}$ mice by administering MOG_{35-55} peptide emulsified in CFA by subcutaneous injection on day 0. Peripheral organs were collected for analyses on 8 dpi.
(B) Flow-based quantification of CD4⁺ T cells in the spleen and peripheral lymph nodes of in WT and *Il3*$^{-/-}$ mice and flow cytometric analysis of CD4⁺ T cell proliferation via Ki67 staining in WT and *Il3*$^{-/-}$ mice (n=7 mice/group).
(C) Flow cytometric analysis of spleen and lymph node CD4⁺ T cell phenotypes based on IFN-γ and IL-17A staining in WT and *Il3*$^{-/-}$ mice (n=7 mice/group).
(D) Flow cytometric analysis of GM-CSF-producing CD4⁺ T cell numbers in WT and *Il3*$^{-/-}$ mice (n=7 mice/group).
(E) Flow cytometry gating strategy and quantification for resident DCs, migratory DC, and moDC populations in lymph nodes (n=7 mice/group).
(F) MFI of MHCII, CD80, CD86, and OX40L among resident DC, migratory DC, and moDC populations in lymph nodes (n=7 mice/group).

(G) Flow cytometry gating strategy and quantification for $CD11b^{-}CD11c^{+}$ and $CD11b^{+}CD11c^{+}$ cells in the spleen (n=7 mice/group).
(H). MFI of MHCII, CD80, CD86, and OX40L among splenic $CD11b^{-}CD11c^{+}$ and $CD11b^{+}CD11c^{+}$ cells (n=7 mice/group).
(I) Schematic of splenocyte *ex vivo* recall response and quantification of $CD4^{+}$ T cells and their positivity for Ki67, IFNγ, and IL-17A at increasing doses of MOG_{35-55} re-stimulation (n=3 mice/group).
(J) Measurement of cytokines in the media of *ex vivo* splenocytes re-stimulated with 20µg MOG_{35-55} (n=3 mice/group).
Mean±s.e.m.
WT, wildtype; MOG, myelin oligodendrocyte glycoprotein; dpi, days post injection; DC, dendritic cell; MFI, mean fluorescence intensity.
Supplemental Figure 2 – related to Figure 1.

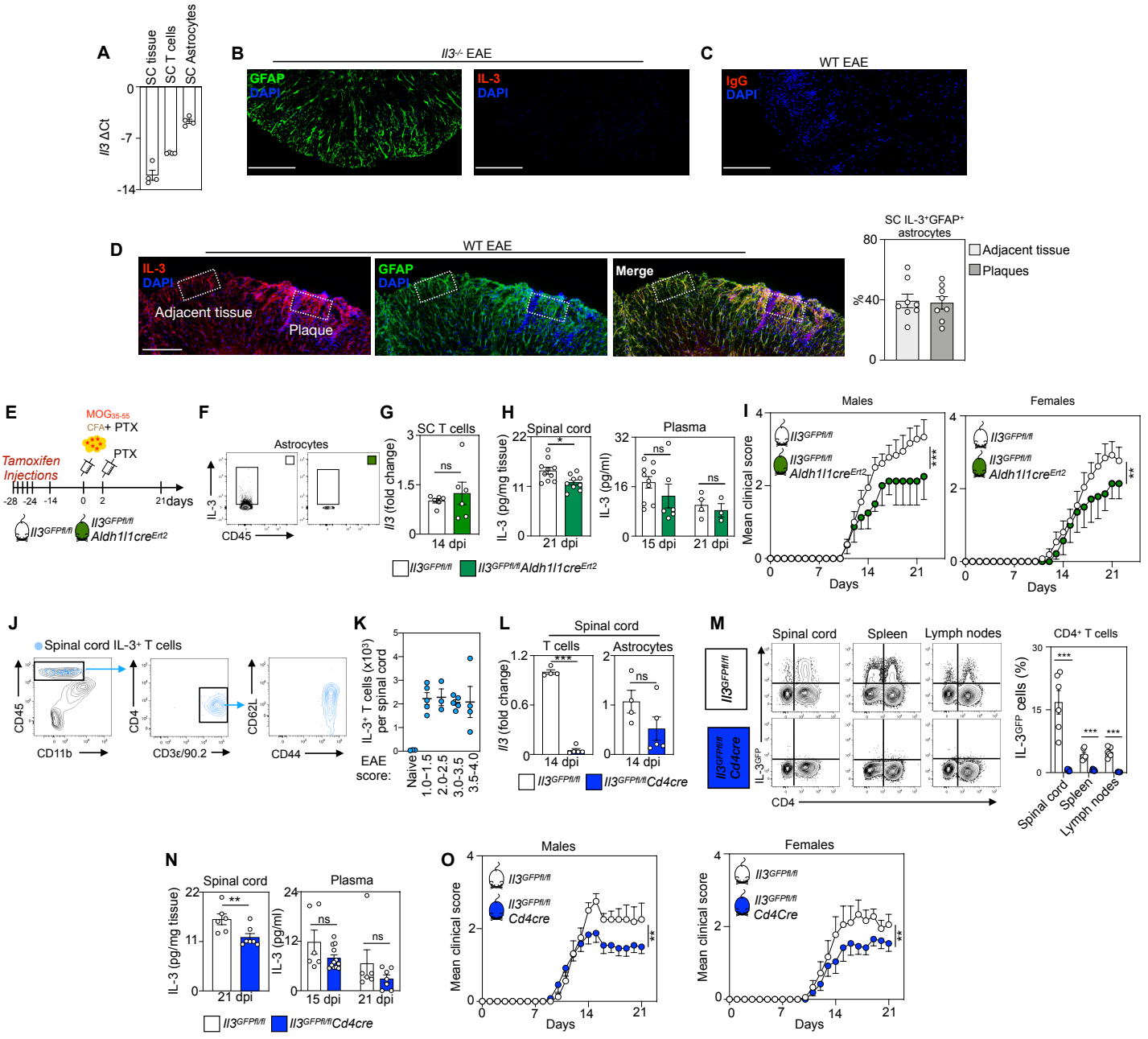

Figure S3. Astrocytes and CD4$^+$ CD44^{hi} effector T_H cells produce IL-3 in the CNS.
(A) *Il3* transcript expression, presented as ΔCt, in SC tissue homogenate and CD44^{hi}CD4$^+$ T cells and astrocytes sorted from the SC of WT mice at peak disease (n=4 mice).
(B) IL-3 and GFAP immunofluorescent staining of *Il3*$^{-/-}$ EAE mice.
(C) Igg control immunofluorescent staining.
(D) Representative image and per cell quantification of IL-3$^+$GFAP$^+$ astrocytes in plaques and adjacent tissue in the SC of WT EAE mice. Scale bars represent 250 µm (8 regions from 3 mice/group).
(E) Strategy of tamoxifen injection and EAE induction in *Il3*$^{GFPfl/fl}$ and *Il3*$^{GFPfl/fl}$*Aldh1l1cre*^{Ert2} mice.
(F) Astrocyte IL-3 in *Il3*$^{GFPfl/fl}$ and *Il3*$^{GFPfl/fl}$*Aldh1l1cre*^{Ert2} mice injected with tamoxifen.
(G) Measurement of *Il3* mRNA expression in CD44^{hi}CD4$^+$ T cells sorted from the SC of *Il3*$^{GFPfl/fl}$ and *Il3*$^{GFPfl/fl}$*Aldh1l1cre*^{Ert2} at peak disease (n=6 mice/group; Mann–Whitney *U*-test).
(H) IL-3 protein abundance in SC homogenates and plasma of diseased *Il3*$^{GFPfl/fl}$ and *Il3*$^{GFPfl/fl}$*Aldh1l1cre*^{Ert2} mice (n=9-10 mice/group; Mann–Whitney *U*-test and two-way ANOVA).
(I) Mean clinical disease scores of male and female *Il3*$^{GFPfl/fl}$ and *Il3*$^{GFPfl/fl}$ *Aldh1l1cre*^{ERT2} mice exposed to EAE (n=9 *Il3*$^{GFPfl/fl}$ males, 4 *Il3*$^{GFPfl/fl}$ *Aldh1l1cre*^{ERT2} males, 13 *Il3*$^{GFPfl/fl}$ females, 7 *Aldh1l1cre*^{ERT2} females; two-way ANOVA).
(J) Characterization and backgating of IL-3-producing T cells in the spinal cord during EAE.

(K) Association of IL-3-producing T cell abundance and disease severity (n=3-5 mice/group).
(L) Measurement of *Il3* mRNA expression in $CD44^{hi}CD4^{+}$ T cells and astrocytes sorted from the SC of $Il3^{GFPfl/fl}$ and $Il3^{GFPfl/fl}CD4cre$ mice at peak disease (n=4-5 mice/group; Mann–Whitney *U*-tests).
(M) Flow cytometry analysis of T cell IL-3 deletion in $Il3^{GFPfl/fl}$ and $CD4creIl3^{GFPfl/fl}$ mice at peak disease (n=4-5 mice/group; one-way ANOVA).
(N) IL-3 protein abundance in SC homogenates and plasma of diseased $Il3^{GFPfl/fl}$ and $Il3^{GFPfl/fl}Cd4cre$ mice (n=6-12 mice/group; Mann–Whitney *U*-test and two-way ANOVA).
(O) Mean clinical disease scores of male and female $Il3^{GFPfl/fl}$ and $Il3^{GFPfl/fl}Cd4cre$ mice exposed to EAE (n= 12 $Il3^{GFPfl/fl}$ males, 8 $Il3^{GFPfl/fl}Cd4cre$ males, 13 $Il3^{GFPfl/fl}$ females, 9 $Il3^{GFPfl/fl}Cd4cre$ females; two-way ANOVA).
Mean±s.e.m., *p<0.05, **p<0.01, ***p<0.001.
ΔCt, delta CT; GFAP, glial fibrillary acidic protein; DAPI, 4′,6-diamidino-2-phenylindole; SC, spinal cord.
Supplemental Figure 3 – related to Figures 2 and 3

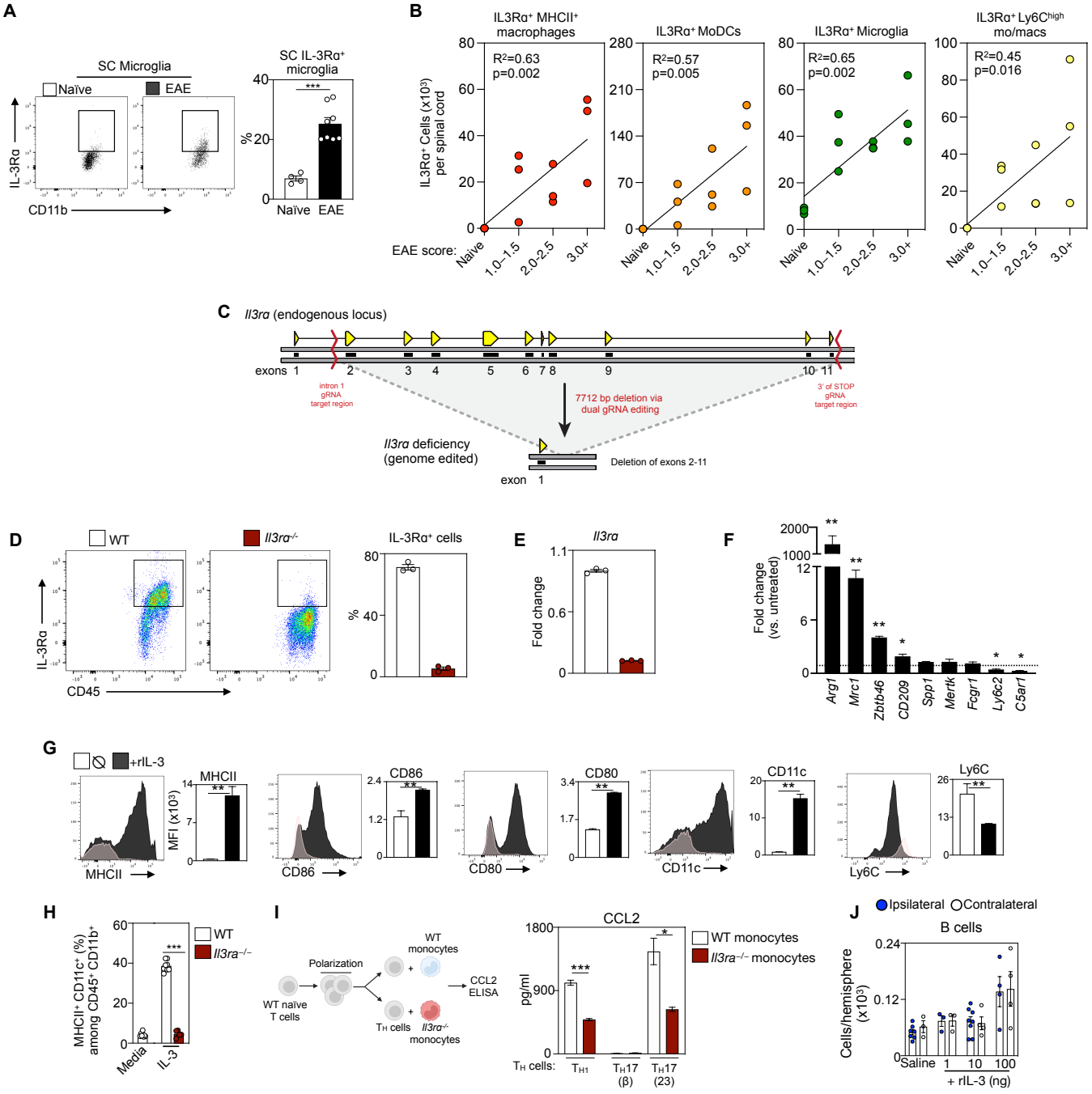

Figure S4. IL-3Rα^{+} myeloid cells and the generation of *Il3ra*$^{-/-}$ mice.
(A) Analysis of IL-3Rα^{+} microglia in the SC of healthy (naïve) and EAE WT mice (n=4-8 mice/group; Mann–Whitney *U*-test).
(B) Analysis of IL-3Rα^{+} cells and disease score (n=2-3 mice/group; Pearson correlation).
(C) Schematic of the endogenous *Il3ra* locus and nuclease-based dual guide RNA (gRNA) editing strategy to generate *Il3ra* knockout mice.
(D) IL-3Rα production by bone marrow monocytes isolated from WT or *Il3ra*$^{-/-}$ mice quantified by flow cytometry.
(E) qPCR analysis of *Il3ra* mRNA expression in BM monocytes isolated from WT or *Il3ra*$^{-/-}$ mice (n=3 mice/group).
(F) Analysis of gene expression for APC-related genes in monocytes stimulated for 24 hr in the presence of rIL-3 (n=3 mice/group; one-way ANOVA).
(G) MFI of MHCII, CD86, CD80, CD11c, and Ly6C^{hi} in monocytes cultures left untreated or stimulated with rIL-3 (n=4-5 mice; Mann–Whitney *U*-tests).

(H) Frequency of MHCII^{+}CD11c^{+} cells among CD45^{+}CD11b^{+} cells in WT and *Il3ra*$^{-/-}$ monocyte culture after stimulation with rIL-3 (n=5-8 mice/group; one-way ANOVA).
(I) Co-culture of polarized T cell subsets with WT or *Il3ra*$^{-/-}$ monocytes and measurement of CCL2 in the media by ELISA (n=3 mice/group; one-way ANOVA).
(J) Enumeration of B cells in the brain of mice 24 hours after stereotactic injection of 0, 1, 10, or 100 ng of rIL-3 (n=3-8 mice/group).
Mean±s.e.m., *p<0.05, **p<0.01, ***p<0.001.
SC, spinal cord; WT, wildtype; EAE, experimental autoimmune encephalomyelitis; BM, bone marrow; rIL-3, recombinant interleukin-3; MFI, Mean fluorescence intensity.
Supplemental Figure 4 – related to Figure 4.

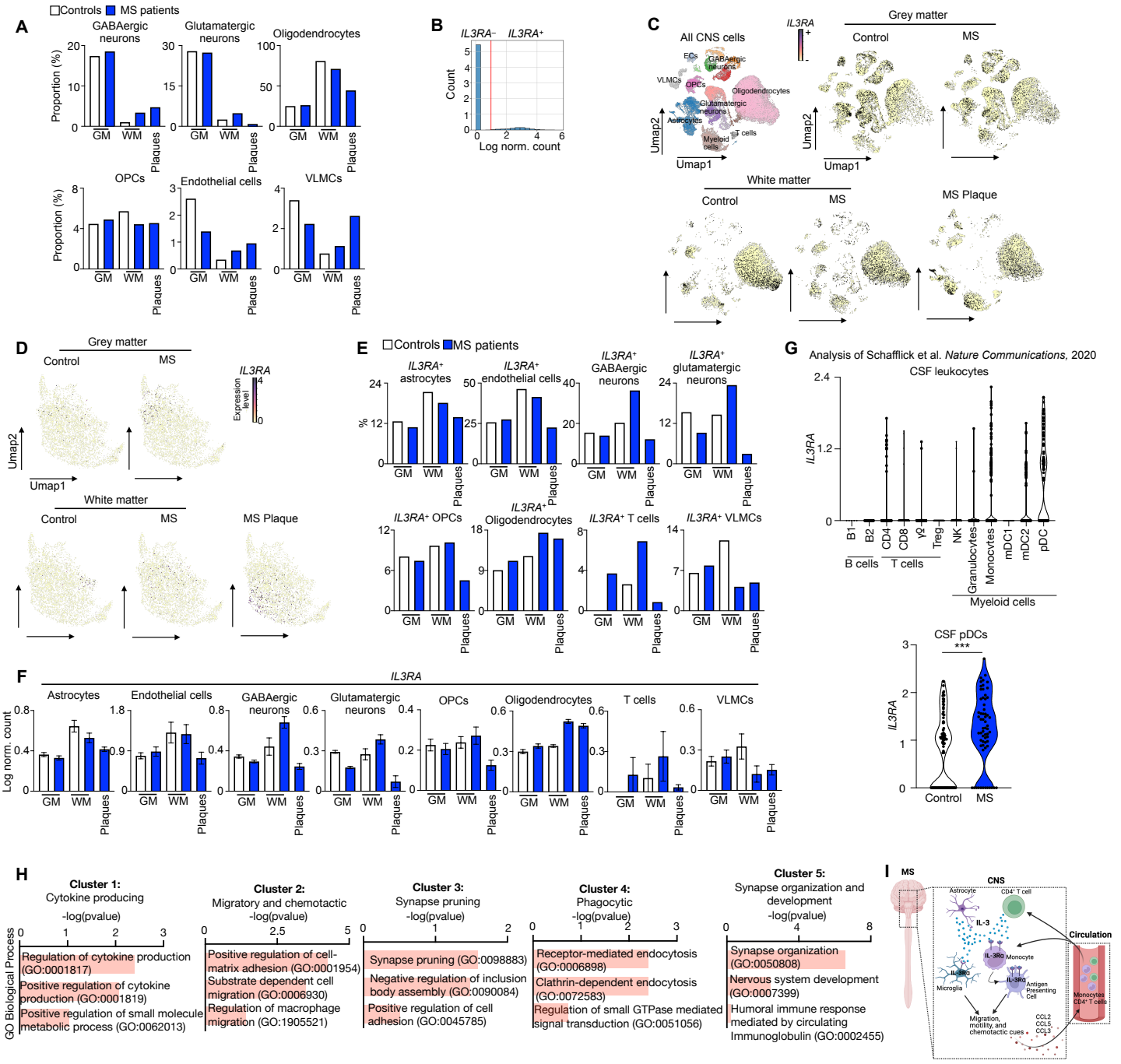

Figure S5. IL-3:IL-3RA signaling in human MS.

(A) Proportion of each CNS cell type across tissue regions and disease states.

(B) Binary strategy to identify *IL3RA* expressing cells.

(C) Umap visualization of *IL3RA* expressing cells in all CNS cells across all regions and conditions.

(D) Umap showing expression of *IL3RA* among myeloid cells in each tissue and condition.

(E) Quantification of IL3RA$^+$ cells among each CNS population across all regions and disease status.

(F) *IL3RA* expression among each CNS population across all regions and disease status.

(G) Analysis of human scRNAseq data of CSF leukocytes from Schafflick et al. 2020 showing expression of *IL3RA* amongst all CSF leukocyte populations in control subjects and *IL3RA* expression in pDCs of control and MS subjects (Mann–Whitney *U*-test).

(H) Pathway analysis of the 5 plaque myeloid cell clusters.

(I) Schematic summarizing the role of astrocyte- and T cell-derived IL-3 promoting monocyte differentiation into APCs and the generation of migratory, motility, and chemotactic cues by resident and peripherally-derived myeloid cells that further recruit monocytes and CD4$^+$ T cells to the CNS.

n=6 unaffected controls and 6 MS patients

Mean±s.e.m. ***p<0.001.

CNS, central nervous system; CSF, cerebrospinal fluid.
Supplemental Figure 5 – related to Figure 5.